Genome Biology

RESEARCH

Open Access

Proteogenomic decoding of chemotherapy resistance in patients with triple-negative breast cancer

Dong Ki Lee[1,2†], Min Hwan Kim[2†], Yumi Hwang[3], Seul-Gi Kim[4], Won-Ji Ryu[3], Geon-Uk Kim[3], Hyun Myoung Yun[3], Shinyoung Park[3], Jeong Dong Lee[3], Hyun Ju Han[3], Gun Min Kim[2], Kyung-Hee Kim[5], Jong Bae Park[6], Min Jung Kim[7], Ja Seung Koo[8], Jee Ye Kim[9], Hyung Seok Park[9], Seung Il Kim[9], Heon Yung Gee[1], Seho Park[9*†] and Joohyuk Sohn[2*†]

[†]Dong Ki Lee and Min Hwan Kim contributed equally to this work.

[†]Seho Park and Joohyuk Sohn jointly supervised this work.

*Correspondence: psh1025@yuhs.ac; oncosohn@yuhs.ac

[2] Division of Medical Oncology, Department of Internal Medicine, Yonsei Cancer Center, Yonsei University College of Medicine, 50-1 Yonsei-ro, Seodaemun-gu, Seoul 03722, Republic of Korea
[9] Division of Breast Surgery, Department of Surgery, Yonsei Cancer Center, Yonsei University College of Medicine, 50-1 Yonsei-ro, Seodaemun-gu, Seoul 03722, Republic of Korea
Full list of author information is available at the end of the article

Abstract

Background: The clinical utility of integrated proteogenomic biomarkers for predicting chemotherapy response in triple-negative breast cancer remains underexplored. We prospectively analyzed paired baseline and post-treatment tumor samples from 50 patients with stage II–III TNBC treated with anthracycline- and taxane-based neoadjuvant chemotherapy, integrating whole-exome sequencing, RNA sequencing, global proteomics, and phosphoproteomics.

Results: Non-negative matrix factorization clustering identifies five proteogenomic subtypes. The immune-enriched subtype demonstrates the highest pathologic complete response rate (55.6%), whereas no pathologic complete response was observed in the xenobiotic metabolism or epithelial–mesenchymal transition subtypes. Immune-related pathways are enriched in tumors with pathologic complete response, while epithelial–mesenchymal transition pathways are enriched in non-pathologic complete response tumors. The estrogen response pathway is selectively enriched in non-pathologic complete response tumors at the proteomic level and inversely correlated with immune activation. Post-translational modification and in vitro analyses suggest estrogen-linked GRK2 activation contributes to chemotherapy resistance. *ITGB8* copy number loss is associated with higher pathologic complete response rates and immune activation, while non-pathologic complete response tumors of the immunomodulatory subtype show increased expression of *AKR1C2* and *ABCA13*. Comparison of baseline and post-treatment tumors reveals AURKB pathway activation in residual disease, with Aurora B kinase inhibition synergizing with paclitaxel. A predictive model incorporating these biomarkers outperforms RNA-based models in predicting response.

Conclusion: Integrative proteogenomic profiling enables robust prediction of chemotherapy resistance in triple-negative breast cancer and identifies actionable biomarkers providing a framework for advancing personalized therapeutic strategies.

Keywords: Triple-negative breast cancer, Neoadjuvant chemotherapy, Proteogenomics, Chemotherapy response, Biomarker

Background

Triple-negative breast cancer (TNBC) is a highly aggressive and clinically challenging breast cancer subtype, characterized by the absence of estrogen receptor (ER), progesterone receptor (PR), and human epidermal growth factor receptor 2 (HER2) expression [1]. TNBC constitutes approximately 10–15% of all breast cancer cases and has high mortality rates and frequent chemotherapy resistance [2]. Owing to the absence of hormone receptors and HER2 expression, patients with TNBC do not benefit from hormonal or HER2-targeted therapies, making cytotoxic chemotherapy the mainstay of systemic treatment [3].

Genomic studies indicate that TNBC rarely harbors recurrent somatic mutations amenable to targeted biologic therapies. Distinct intrinsic molecular subtypes have been defined based on mRNA expression profiles, such as Lehmann classification [4–6]. Notably, several clinical studies have suggested correlations between these molecular subtypes and therapeutic responses, including IMpassion 130 and CIBOMA trials [7, 8]; however, the ASCO clinical guideline currently recommends no molecular biomarker to reliably predict chemotherapy response in patients with early-stage TNBC due to insufficient evidence [9]. Moreover, observed clinical outcomes often conflict with proposed subtype pathogenesis [10]. For example, adjuvant platinum chemotherapy failed to demonstrate clinical benefit in basal-like TNBC in EA1131 study and androgen receptor antagonists yielded little activity in luminal androgen receptor (LAR) subtype [11, 12]. Recent advancements have led to the approval of novel molecularly targeted therapies, including immune checkpoint inhibitors (anti-PD-1/PD-L1 blockade) and antibody–drug conjugates targeting trophoblast cell surface antigen 2 (TROP2) or HER2 [13, 14]. Nevertheless, the prognosis remains poor for those with recurrent or metastatic TNBC, underscoring the urgent need for improved strategies to prevent recurrence and guide treatment.

The KEYNOTE-522 trial established neoadjuvant chemotherapy comprising pembrolizumab combined with paclitaxel and carboplatin, followed by anthracycline and cyclophosphamide before surgery as the standard of care for patients with stage II–III TNBC [15–18]. Notably, pembrolizumab exhibits therapeutic benefit only when combined with chemotherapy, reinforcing the role of anthracycline–taxane-based cytotoxic chemotherapy as the backbone of early- and advanced-stage TNBC treatment. Despite ongoing research, existing biomarkers, including PD-L1 and homologous recombination deficiency, have shown limited predictive value for chemotherapy response in clinical practice [19–21]. Therefore, alternative approaches, such as mass spectrometry (MS)-based proteomic and phosphoproteomic analyses, hold promise to better characterize baseline and residual tumors on neoadjuvant chemotherapy and to identify predictive biomarkers for therapeutic response. Herein, we aimed to identify molecular factors associated with chemotherapy response and resistance through a comprehensive

proteogenomic analysis of patients with stage II–III TNBC treated with neoadjuvant chemotherapy, using matched baseline core biopsies and residual surgical tumor tissues.

Results

Patient cohort and proteogenomic analysis

Comprehensive proteogenomic analyses were conducted in 50 patients with TNBC treated with neoadjuvant chemotherapy using matched whole-exome sequencing (WES), RNA sequencing (RNA-seq), and tandem mass tag (TMT)-based MS for global and phosphoproteomic tumor profiling (Additional file 1: Fig. S1, S2A). The median age of patients was 48 years, with most presenting with clinical T2 stage (92%) and node-negative (N0) disease (58%) (Additional file 1: Table S1). The proteogenomic pathway analysis was performed on baseline tumors from 41 patients with complete baseline WES, RNA-seq, and TMT-MS datasets, and pre- and post-treatment tumor comparison analysis was performed for patients with matched protein TMT data ($n=22$). At surgical pathology evaluation, 38% of patients ($n=19$) achieved a pathological complete response (pCR). Progression during chemotherapy occurred in six (12%) patients and disease recurrence in seven (14%), with a median follow-up duration of 33.2 months (Additional file 1: Fig. S2B). Tumor purity estimates derived from RNA and proteomic data were highly correlated (Additional file 1: Fig. S2C). Overall, RNA and protein expression levels exhibited a moderate correlation; 93.8% of genes showed positive correlations, and 62.0% of these were significant ($P<0.01$), particularly among the genes involved in glucose, amino acid, and fatty-acid metabolism (Additional file 1: Fig. S2D, E). However, several gene sets demonstrated notable discrepancies between RNA and protein expression, including ribosome, oxidative phosphorylation, basal transcription factors, RNA polymerase, and spliceosome pathways (Additional file 1: Fig. S2E).

Comprehensive NMF clustering of patients with TNBC

We delineated molecular subtypes within the TNBC cohort through NMF clustering using an integrated multi-omics dataset, including copy number alterations (CNAs), transcriptomic expression, protein, and phosphoprotein expression derived from baseline tumor samples (Fig. 1A). This analysis identified five distinct clusters with unique molecular features: "immune-enriched" ($n=9$), "xenobiotic metabolism" ($n=2$), "epithelial-mesenchymal transition (EMT)" ($n=7$), "MYC-dependent" ($n=12$), and "mesenchymal with estrogen signature" ($n=11$) (Fig. 1A).

To evaluate how these proteogenomic clusters relate to established transcriptomic classifications, we applied both the Lehmann and Fudan TNBC subtype classification [6, 22]. These proteogenomic subtypes did not align with the Lehmann classification, with marked discrepancies observed in clusters 3, 4, and 5 (Fig. 1B). Comparison with the Fudan classification showed that clusters 3 and 4 exhibited mixed subtype composition, containing BLIS, mesenchymal, and IM subtypes (Additional file 1: Fig. S3).

Evaluation of treatment response revealed that the "immune-enriched" cluster demonstrated the highest pCR rate (55.6%; five of nine patients), while no pCRs were observed in the "xenobiotic metabolism" or "EMT" clusters (Fig. 1C). These findings suggest a strong influence of proteogenomic profiles on response to neoadjuvant chemotherapy. To further characterize the molecular programs underlying each cluster, we performed

Fig. 1 Comprehensive NMF clustering of patients with TNBC. **A** Heatmap illustrating comprehensive NMF clustering analysis using integrated datasets, including gene mutations, CNAs, RNA expression, and global and phosphoprotein expression profiles derived from baseline tumor tissues. Annotation tracks indicate the Lehmann classification, NMF clusters, and treatment response (pCR, non-pCR, and progression). For each molecular layer (RNA, protein, and phosphoprotein), representative Hallmark pathways enriched among differentially expressed genes are listed. Five distinct NMF clusters were identified: "immune-enriched" ($n = 9$), "xenobiotic metabolism" ($n = 2$), "EMT" ($n = 7$), "MYC-dependent" ($n = 12$), and "mesenchymal with estrogen signature" ($n = 11$). **B** Comparison of NMF-derived proteogenomic clusters with the RNA-seq-based Lehmann classification. **C** Bar plot showing pCR rates of patients with TNBC according to the NMF clusters. **D** Hallmark GSVA based on proteomic data, showing representative pathway enrichment patterns across NMF clusters, with clustering based on immune activation, cell cycle, metabolism, and EMT-related signatures. **E** Oncogenic signature (C6) GSVA based on proteomic data, showing distinct pathway enrichment patterns across NMF clusters. **F** Proportion of patients with germline BRCA1 or BRCA2 mutations in NMF clusters. See also Figure S2, S3, S4, and S5. EMT, epithelial-to-mesenchymal transition; NMF, non-negative matrix factorization; pCR, pathological complete response

Hallmark gene set variation analysis (GSVA) based on both RNA and protein expression data. Cluster 1 showed enrichment of interferon (IFN) response and inflammatory pathways, cluster 3 demonstrated activation of EMT and angiogenesis, and cluster 4 exhibited upregulation of E2F and MYC target pathways (Fig. 1D). Comparison of omics layers revealed that proteome-based GSVA results displayed higher inter-cluster variability (SD = 0.2449) than RNA-based GSVA (SD = 0.1162; $P = 7.77 \times 10^{-16}$, Additional file 1: Fig. S4A, B). In oncogenic signature (C6) GSVA analysis, cluster 4 showed E2F1 and MYC signature upregulation (Fig. 1E), and STK33 signature upregulation was noted in the tumors of clusters 1, 2, and 3. For DNA-level comparison, the clusters 2 and 3 were devoid of germline BRCA1/2 mutations, in contrast to the other clusters (Fig. 1F). Otherwise, no significant differences were identified in genomic alterations or CNAs across the clusters, despite the observed diversity in transcriptomic and proteomic characteristics.

To externally validate the clinical and biological relevance of our proteogenomic TNBC classification, we applied the transcriptomic signatures derived from each of the five NMF-defined clusters to an independent cohort from the METABRIC study (n = 258) [23]. Differentially expressed genes (adjusted $P < 0.05$ and $|\log_2$ fold change$| > 1$) specific to each NMF cluster in our cohort were used for k-means clustering of the METABRIC TNBC samples (Additional file 1: Fig. S5A). Of these, 197/258 tumors (76.3%) were assigned to one of the five clusters in accordance with our multi-omics analysis. Relapse-free survival analysis showed prognostic relevance of the classification also in the METABRIC cohort, with Cluster 1 associated with the most favorable outcome and Cluster 5 with the poorest prognosis (Additional file 1: Fig. S5B). Together, these findings demonstrate that our NMF-based proteogenomic classification is reproducible in METABRIC datasets.

GSEA for predictors of pCR in patients with TNBC

We evaluated the molecular pathways associated with chemotherapy response in TNBC using RNA-seq and TMT-based proteomic data (Fig. 2A). Hallmark pathway GSVA revealed a consistent enrichment of EMT signatures in non-pCR tumors across transcriptomic and proteomic datasets. In contrast, tumors from patients who achieved pCR demonstrated upregulation of immune-related pathways, including IFN-α response, IFN-γ response, allograft rejection, and inflammatory response, as well as cell cycle-related pathways, such as E2F targets and G2M checkpoint signaling. These findings align with those of prior studies linking elevated immune infiltration and activity with improved chemotherapy response, while EMT and transforming growth factor (TGF)-β pathway activation have been associated with treatment resistance [24, 25].

Gene set enrichment analysis (GSEA) comparing patients with and without disease recurrence further supported these observations. Recurrent tumors were enriched for myogenesis and EMT pathways (Fig. 2B). Notably, several gene sets associated with poor treatment response, including the estrogen response pathway, were preferentially identified in proteomic data but not in RNA-seq analyses (Fig. 2C, Additional file 1: Fig. S6A). Although estrogen response signatures were generally low across the cohort, differential proteomic analysis identified a subset of estrogen response genes, including DHRS2, SLC26A2, CLIC3, DHCR7, and HSPB8, that were higher in

non-pCR tumors (Fig. 2D, Additional file 1: Fig. S6B). When patients were stratified by estrogen response GSVA score, those with higher scores exhibited significantly lower pCR rates (14.3% vs 48.1%, $P = 0.0328$; Additional file 1: Fig. S6C). Estrogen signatures were higher in clusters 2, 3, and 5 than in clusters 1 and 4 (Additional file 1: Fig. S6D, E). Estrogen signaling has been previously implicated in immune suppression across malignancies [26, 27]. In our analysis, estrogen signature expression was negatively associated with the ESTIMATE immune score, indicating reduced immune activity (Fig. 2E, Additional file 1: Fig. S6F). Moreover, although correlations were weak, estrogen response signatures were significantly inversely correlated with G2M checkpoint signature and positively correlated with EMT signature, suggesting that tumors exhibiting estrogen pathway activation have a modest tendency for low-proliferative and EMT properties (Fig. 2E, Additional file 1: Fig. S6G). These results suggest that proteome-level upregulation of estrogen response, undetectable at the RNA level, contributes to neoadjuvant chemotherapy resistance in patients with TNBC. Additionally, protein GSVA analysis using C6 oncogenic signatures showed that *KRAS, ERBB2*, and *PTEN*-downregulation signatures are upregulated in non-pCR patients, consistent with their contribution to TNBC pathogenesis (Fig. 2F).

To validate the association between estrogen signaling and chemotherapy response, we analyzed two independent TNBC proteogenomic datasets. In the Anurag et al. TNBC cohort [25], tumors with higher estrogen response GSVA scores (enrichment score > 0.1) exhibited a trend toward lower pCR rates, although the difference did not reach statistical significance ($P = 0.5585$; Additional file 1: Fig. S7A). In the Gong and Jiang et al. TNBC cohort [28], patients with high estrogen response GSVA scores showed significantly shorter relapse-free survival compared with those with low scores ($P = 0.0438$; Additional file 1: Fig. S7B). These external validations support the prognostic relevance and potential role of proteome-level estrogen pathway activation in TNBC.

(See figure on next page.)

Fig. 2 Pathway signatures associated with chemotherapy response and recurrence in patients with TNBC. **A** Hallmark pathway enrichment analysis comparing non-pCR versus pCR tumors using RNA-seq and global protein TMT data. Pathways are plotted based on the $-\log_{10}$(FDR) values derived from RNA and protein GSEA. Pathways enriched in the non-pCR group are shown on the positive axis (RNA: right on the x-axis; protein: up on the y-axis), whereas those enriched in the pCR group are displayed on the negative axis (RNA: left on the x-axis; protein: down on the y-axis). Significance is represented by $-\log_{10}$(FDR); color indicates statistical significance in RNA only (purple), protein only (yellow), or both (blue). **B** Hallmark pathway enrichment analysis of RNA-seq and proteomic data comparing tumors from patients with disease recurrence versus those without recurrence. Pathways enriched in the recurrence group are plotted on the positive axis (RNA: right on the x-axis; protein: up on the y-axis), whereas those enriched in the disease-free group appear on the negative axis (RNA: left on the x-axis; protein: down on the y-axis). **C** Bar plot illustrating significantly enriched signaling pathways identified by protein-based GSEA (defined by FDR < 0.05). Pathways enriched in non-pCR tumors are indicated in red, while pathways enriched in pCR tumors are in green. Estrogen response pathways are highlighted in orange. **D** Heatmap displaying protein expression of genes within the early estrogen response signature, comparing non-pCR and pCR tumors. The top 20 genes with the highest expression in non-pCR tumors are shown. Asterisks (*) denote statistically significant differences ($P < 0.05$). **E** Correlation analysis between protein GSVA estrogen early response signature and the ESTIMATE immune score (left), G2M checkpoint signature (middle), and epithelial-mesenchymal transition (right), respectively. The R^2 and p-values are calculated using Pearson's correlation test. **F** Heatmap showing GSVA data of C6 oncogenic signature gene sets in pCR and non-pCR tumors. *$P < 0.05$ by Student's t test with Welch's adjustment for heteroscedasticity (D) or by Pearson's correlation (E). See also Figure S6. EMT, epithelial-to-mesenchymal transition; FDR, false discovery rate; GSEA, gene set enrichment analysis; GSVA, gene set variation analysis; pCR, pathological complete response

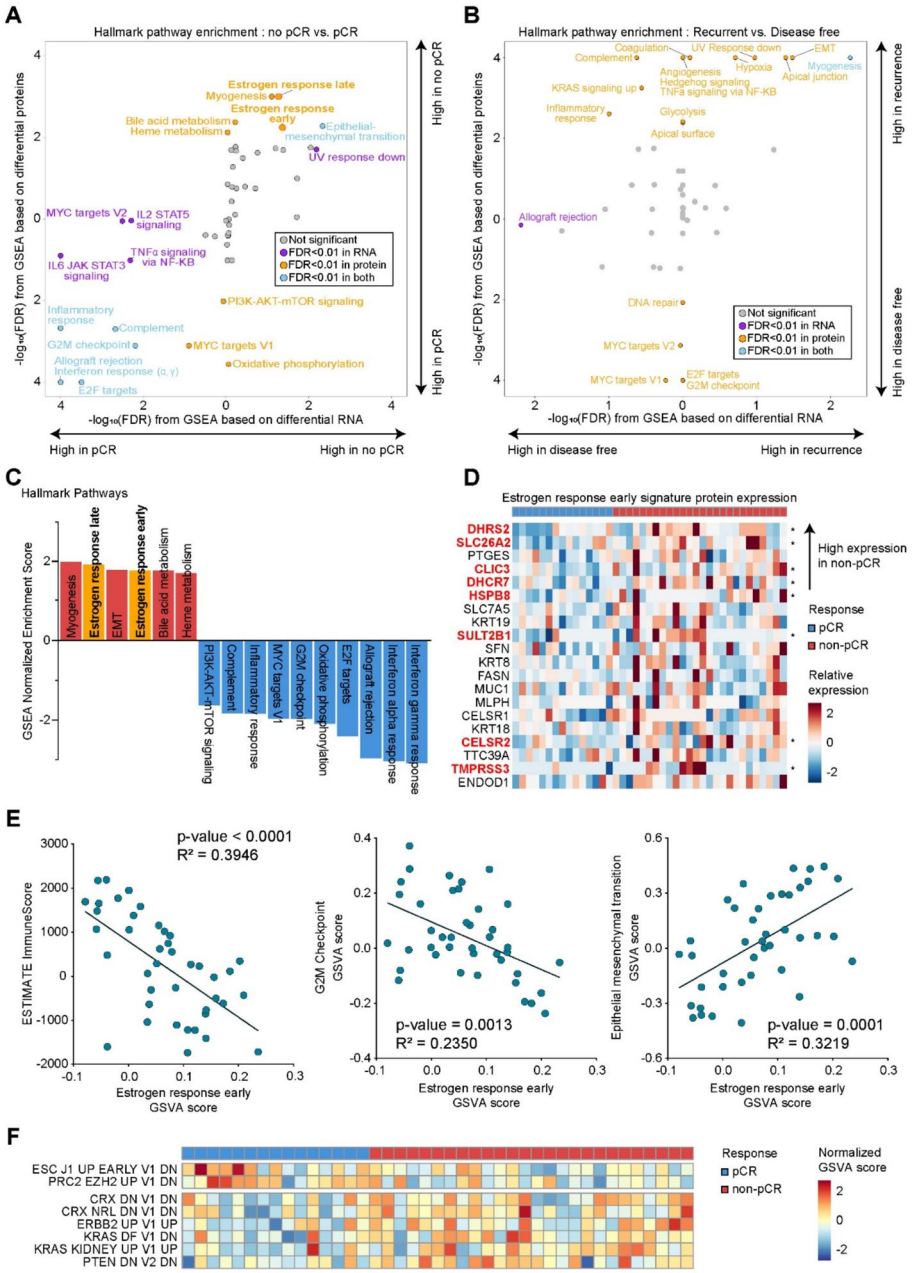

Fig. 2 (See legend on previous page.)

PTM signature predicts chemotherapy response

Next, we analyzed the post-translational modification (PTM) signatures to explore their association with neoadjuvant chemotherapy response in TNBC. PTM-set enrichment analysis (PTM-SEA) revealed significant enrichment of GRK2 and GRK5 signaling in non-pCR tumors, whereas GSK3β signaling and immune-related pathways, including IL2 and CCR7, were predominantly enriched in pCR tumors (Fig. 3A). Prior evidence indicates that estrogen signaling can induce GRK2 activation in various biological contexts [29, 30]. Consistent with these findings, the GRK2 PTM signature positively correlated with estrogen response signatures and negatively correlated with the ESTIMATE

immune score (Fig. 3B–D). The phosphoprotein expression profiles of GRK2 downstream pathway genes, including PRKRA, SQSTM1, and G3BP2, were upregulated in tumors of non-pCR patients (Fig. 3E). Further pathway analysis comparing GRK2-high (normalized enrichment score [NES] > 2) versus GRK2-low tumors revealed higher estrogen response in GRK2-high tumors, while immune-related signatures like allograft rejection and IFN alpha/gamma response pathways were higher in the GRK2-low tumors, which were previously implicated in chemotherapy resistance and immunosuppression in TNBC (Fig. 3F) [31–33]. We validated the functional role of GRK2 through *invitro* assays, demonstrating that estradiol treatment increased GRK2 levels in MDA-MB468 TNBC cells (Fig. 3G). Pharmacological inhibition by GRK2 (βARK) inhibitor also significantly enhanced paclitaxel sensitivity in the MDA-MB-231 cell line (Fig. 3H). Combination treatment with varying doses of GRK2 (βARK) inhibitor and paclitaxel in MDA-MB-231 cells resulted in synergistic inhibition of cell viability (Bliss synergy score 8.08, Additional file 1: Fig. S8). These findings suggest a potential association between GRK2 activation and chemotherapy resistance in TNBC that warrants further mechanistic investigation.

ITGB8 loss predicts favorable neoadjuvant chemotherapy response

To examine the impact of gene CNAs and corresponding protein expression changes on chemotherapy response in TNBC, we performed cytoband enrichment analysis. We aimed to identify CNA regions associated with upregulated genes in tumors exhibiting either pCR or non-pCR in both transcriptomic and proteomic datasets (Additional file 1: Fig. S9A). Cytoband-based GSEA demonstrated that several regions exhibited coordinated amplification and upregulation of gene expression in non-pCR tumors, with the most prominent enrichment observed at chromosome 7p21 in both RNA and protein datasets (Fig. 4A, Additional file 1: Fig. S9B, C). We intersected the core enrichment

(See figure on next page.)

Fig. 3 Estrogen-*GRK2* pathway and its functional implications in TNBC chemoresistance. **A** Volcano plot showing enriched PTM pathways between the pCR and non-pCR groups by PTM-SEA. The x-axis represents the NES, and the y-axis shows the -$\log_{10}$(*p*-value). Only pathways meeting the significance threshold (|NES|> 5 and *p*-value < 0.05) are color-coded (red: NES > 5 and blue: NES < −5), whereas nonsignificant pathways are shown in gray. **B** Correlation analysis between the GRK2 PTM-SEA NES and early estrogen response GSVA scores. **C** Correlation analysis between the GRK2 PTM-SEA NES and late estrogen response GSVA scores. **D** Correlation analysis between the GRK2 PTM-SEA NES and ESTIMATE immune scores. **E** Heatmap of in vitro kinase-to-phosphosite database (iKiP) GRK2 pathway-associated phosphosites used in the PTM-SEA analysis. Asterisks (*) denote statistically significant differences ($P < 0.05$) between the pCR and non-pCR group. **F** GSVA comparison of Hallmark pathways between GRK2 PTM-SEA score–high and score–low tumors. Estrogen response early ($P = 0.0324$) and allograft rejection ($P = 0.0310$) were significantly different, with estrogen response early and late pathways enriched in the GRK2-high group, whereas allograft rejection and interferon alpha/gamma response were higher in the GRK2-low group. Data are presented as mean ± SD. **G** Immunoblot showing GRK2 protein expression on estradiol treatment for 24 h in MDA-MB468 cell line. Protein size markers were indicated on the right side of the immunoblots. **H** Dose–response curve of relative proliferation of MDA-MB231 cells treated with paclitaxel and GRK2 inhibitor (βARK inhibitor, 4 μg/ml [15.2 nM]) plus paclitaxel in the *in-vitro* 3-(4,5-dimethylthiazol-2-yl)−2,5-diphenyltetrazolium bromide (MTT) assay. The x-axis is $\log_{10}$ (paclitaxel concentration). The results are from three biologic replicates, and the error bars indicate the standard error of the mean (SEM). *$P < 0.05$ by Student's t test with Welch's adjustment for heteroscedasticity (E) or by Pearson's correlation (B, C, and D). See also Figure S8. GRK2i, GRK2 inhibitor; GSVA, gene set variation analysis; iKiP, in vitro kinase-to-phosphosite; NES, normalized enrichment score; pCR, pathological complete response; PTM, post-translational modification; PTM-SEA, post-translational modification set enrichment analysis

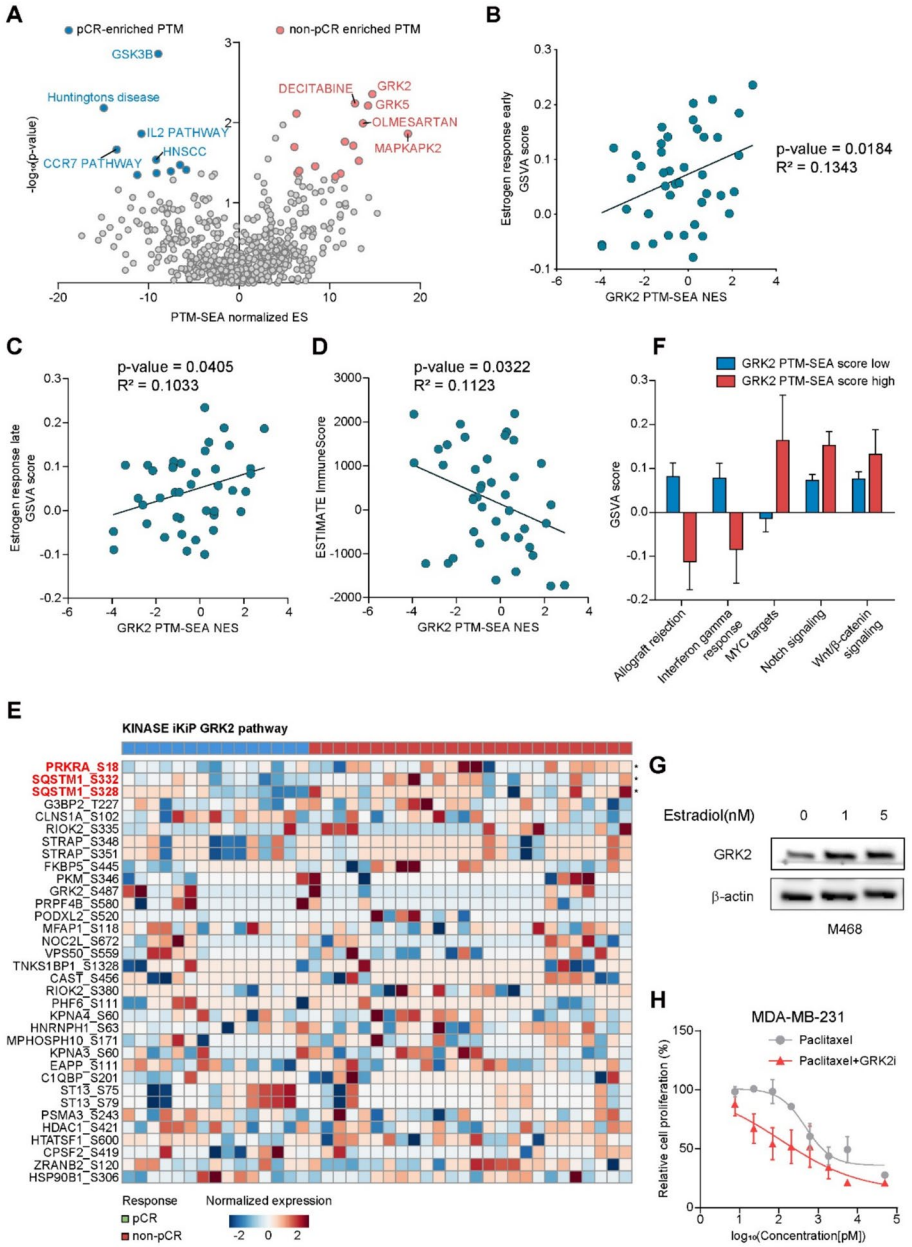

Fig. 3 (See legend on previous page.)

genes from 7p21 with curated cell-surface proteins from the Cancer Surfaceome Atlas [34], to further refine candidate genes targetable by antibodies or antibody–drug conjugates. This integrative analysis revealed three overlapping genes: *ITGB8*, *THSD7A*, and *TSPAN13* (Fig. 4B). Among them, *ITGB8* exhibited the highest CNA difference between pCR and non-pCR tumors, prompting its selection for further evaluation, and ITGB8 was one of the most overexpressed integrin genes in non-pCR tumors (Additional file 1: Fig. S10A).

ITGB8 can suppress anti-tumor immunity via TGF-β signaling in colorectal and breast cancers, and its genetic loss induces autoimmune-like phenotypes in mouse models,

suggesting a tumor-suppressive role for the ITGB8-TGFβ axis in TNBC [35–37]. *ITGB8* RNA and protein expression levels correlated with *ITGB8* copy number (Additional file 1: Fig. S10B, C), and an inverse relationship was observed between *ITGB8* copy number and pCR rates; specifically, patients exhibiting *ITGB8* loss in both copies had a pCR rate of 80.0%, while those exhibiting a single copy gain of *ITGB8* had a pCR rate of 0% (80.0% vs. 41.7% vs. 12.6% vs. 0.0%, $P = 0.036$; Fig. 4C). Consistently, tumors with *ITGB8* loss demonstrated upregulation of the IFN-α and IFN-γ response pathways and downregulation of the E2F and G2M checkpoint signatures in GSEA analyses (Fig. 4D). PTM-SEA further revealed enrichment of activated T cell-associated protein signatures, such as *IL-3* and *CCR7* pathways, in tumors with *ITGB8* loss compared to tumors without *ITGB8* copy loss (Fig. 4E). Tumors exhibiting *ITGB8* gain also showed a low ESTIMATE immune score, suggesting lower immune cell infiltration (Additional file 1: Fig. S10D).

To experimentally validate the transcriptional consequences of ITGB8 gain, we performed RNA-sequencing in MDA-MB-468 cells overexpressing ITGB8 (ITGB8-OE) compared with mock (pEGFP)-transfected controls. GSVA of Hallmark pathways revealed that ITGB8 overexpression led to broad downregulation of inflammatory and immune response programs, including TNF-α signaling via NF-κB, IFN-α response, and IFN-γ response (Additional file 1: Fig. S11A). Consistent with these results, GSEA showed significantly negative enrichment for IFN-α response (NES = −1.73, FDR = 0.0050), IFN-γ response (NES = −2.31, FDR < 0.0001), inflammatory response (NES = −2.52, FDR < 0.0001), and TNF-α signaling via NF-κB (NES = −3.06, FDR < 0.0001) in ITGB8-OE cells relative to control (Additional file 1: Fig. S11B). These findings show that ITGB8 activation can transcriptionally repress immune and inflammatory signaling.

Finally, validation using the TCGA TNBC cohort data showed improved overall survival for patients with *ITGB8* copy number loss compared with that of patients without loss, supporting the prognostic relevance of *ITGB8* genomic alterations (Fig. 4F) [38]. These results suggest that changes in *ITGB8* copy number modulate anti-tumor immune responses in TNBC through the ITGB8-TGFβ axis.

(See figure on next page.)

Fig. 4 *ITGB8* CNAs and their association with chemotherapy response of TNBC. **A** Bar plot showing enrichment scores in the cytoband-based GSEA identifying chromosome 7p21 overlapping in transcriptomic and proteomic data. **B** Venn diagram showing the overlap between core enrichment genes from the 7p21 cytoband identified in transcriptomic and proteomic datasets and surface proteins curated from the Cancer Surfaceome Atlas. *ITGB8*, *THSD7A*, and *TSPAN13* were shared across all datasets, with *ITGB8* exhibiting the highest copy number difference between pCR and non-pCR tumors. **C** Bar plot showing pCR rates according to the *ITGB8* copy number status. **D** Hallmark pathway enrichment analysis comparing tumors with *ITGB8* copy number loss versus those without loss using RNA-seq and tandem mass tag (TMT)-based global proteomic data. Pathways are plotted according to their $-\log_{10}$(FDR) values derived from RNA- and protein-level GSEA. Pathways enriched in the *ITGB8* loss group are shown on the positive axis (RNA: right on the x-axis; protein: up on the y-axis), whereas those enriched in the no-loss group are displayed on the negative axis (RNA: left on the x-axis; protein: down on the y-axis). Significance is represented by $-\log_{10}$(FDR); color indicates statistical significance in RNA only (purple), protein only (orange), or both (blue). **E** Volcano plot showing enriched PTM pathways comparing the tumors with *ITGB8* copy number loss versus no loss. **F** Kaplan–Meier survival analysis for overall survival according to the *ITGB8* copy number in the TCGA TNBC cohort ($n = 154$). The P-value was calculated using the log-rank test. See also Figure S9, S10, and S11. CN, copy number; GSEA, gene set enrichment analysis; NES, normalized enrichment score; pCR, pathological complete response; PTM, post-translational modification

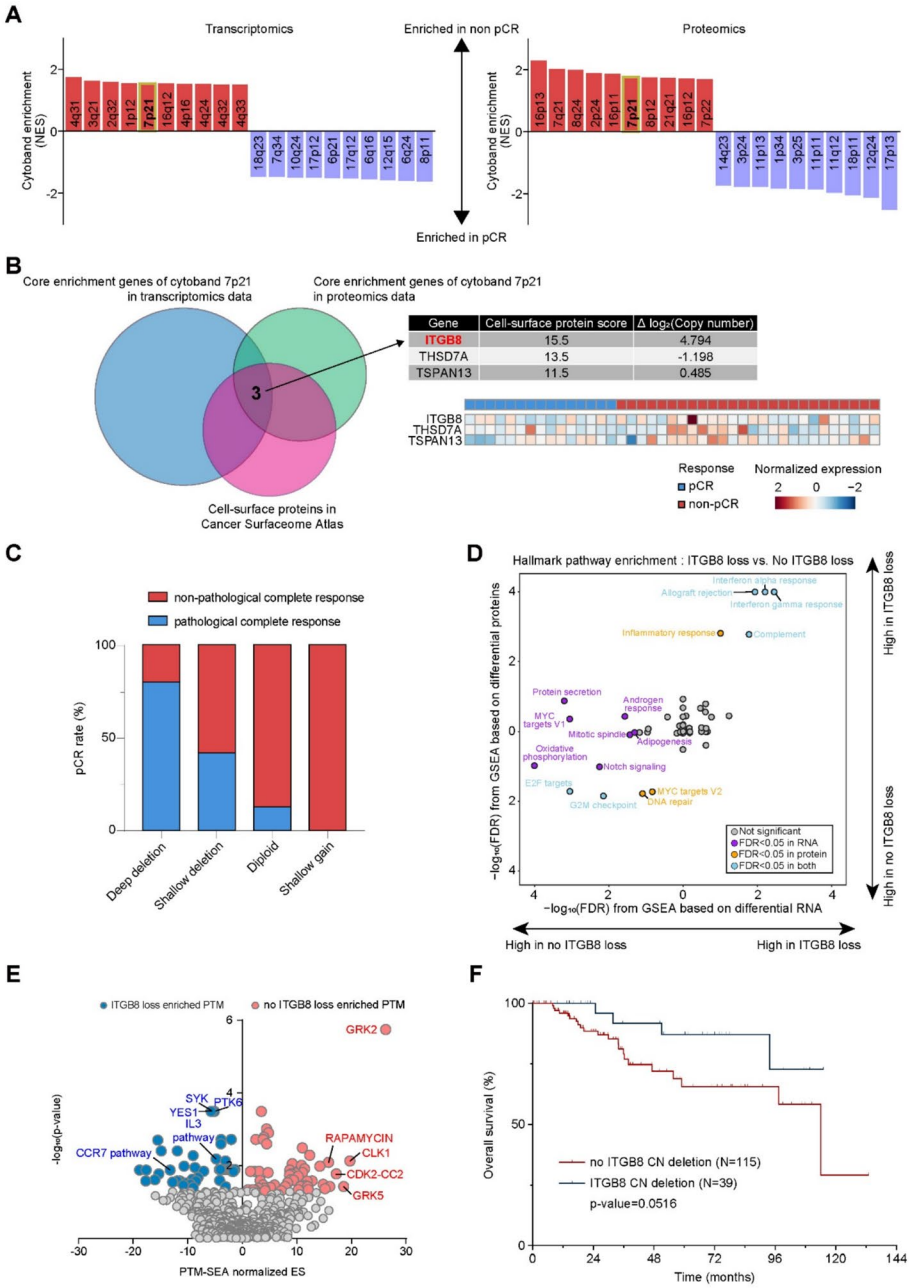

Fig. 4 (See legend on previous page.)

Doxorubicin metabolism and drug efflux gene upregulation as resistance mechanisms

pCR was associated with elevated immune-related signatures; however, a substantial proportion of patients classified within the Lehmann IM subtype (36.8%) did not achieve pCR. To investigate potential resistance mechanisms in this group, we analyzed transcriptomic and proteomic data of the IM subtype. At the transcriptomic-level, we identified significant mRNA upregulation of *AKR1C2*, a member of the aldo–keto reductase family involved in doxorubicin metabolism, and *ABCA13*, an ATP-binding cassette transporter linked to drug efflux, in non-pCR patients (Fig. 5A). These genes

have previously been implicated in chemotherapy resistance and poor survival outcomes in other malignancies, such as ovarian cancer [39, 40]. Next, we examined *AKR1C2* and *ABCA13* expression across the five NMF-defined TNBC clusters. *AKR1C2* was most highly expressed in cluster 2, characterized by xenobiotic response pathways, and *ABCA13* was enriched in clusters 4 and 5 (Fig. 5B). A heatmap integrating transcriptomic and proteomic data confirmed consistent expression of xenobiotic metabolism genes across these clusters (Fig. 5C, Additional file 1: Fig. S12A).

To validate these findings in an independent cohort, we examined *AKR1C2* and *ABCA13* expression in the METABRIC TNBC IM subtype cohort (n = 58). Elevated *AKR1C2* expression was significantly associated with worse relapse-free survival (RFS; $P = 0.0033$; Additional file 1: Fig. S7C). *ABCA13* expression showed a trend toward worse survival in the high expression group within the METABRIC IM cohort, but this association did not reach statistical significance ($P = 0.2225$; Additional file 1: Fig. S7D). Collectively, these findings suggest that upregulation of drug metabolism and efflux pathways, particularly through AKR1C2 and ABCA13, contributes to chemotherapy resistance in immune-enriched TNBC tumors.

Proteogenomic comparison of baseline and post-treatment tumors reveals AURKB as a candidate resistance target

We next evaluated molecular adaptations associated with resistance to neoadjuvant chemotherapy through a paired analysis of baseline and residual (post-treatment) tumor samples ($n = 22$). GSEA of proteomic data revealed the enrichment of EMT and myogenesis signatures in residual tumors after neoadjuvant chemotherapy (Fig. 5D). Differential gene expression analysis further showed upregulation of EMT, myogenesis, and xenobiotic metabolism pathway genes in residual tumors (Protein: Fig. 5E, Additional file 1: Fig. S12B, RNA: Additional file 1: Fig. S12C). PTM-SEA revealed enrichment of key phosphoprotein signaling signatures, including CGK2, Aurora kinase B (AURKB), and MAP3K3, in post-treatment tumors (Fig. 5F).

(See figure on next page.)

Fig. 5 Identification of chemotherapy resistance mechanisms in the IM subtype and baseline and post-treatment tumor comparison. **A** Volcano plot showing differentially expressed mRNAs between non-pCR and pCR tumors in the Lehmann classification IM subtype. **B** Violin plot showing mRNA expression levels of *AKR1C2* and *ABCA13* stratified by the five NMF clusters. **C** Heatmap comparing mRNA expression of xenobiotic metabolism genes across the TNBC cohort. **D** Hallmark pathway enrichment analysis comparing baseline versus post-treatment samples using phosphoproteomic and global proteomic data. Pathways are plotted according to their $-\log_{10}$(FDR) values derived from GSEA of phosphoprotein expression (x-axis) and protein expression (y-axis). Pathways enriched in the post-treatment group are shown on the positive axis (phosphoprotein: right on the x-axis; protein: up on the y-axis), whereas those enriched in the baseline group appear on the negative axis (phosphoprotein: left on the x-axis; protein: down on the y-axis). Significance is represented by $-\log_{10}$(FDR); color indicates statistical significance in the protein layer only (orange) or in both phosphoprotein and protein layers (blue). **E** Bar plot showing the enriched Hallmark pathways in DEGs between post-treatment and baseline samples in global protein expression data. The top five gene signatures are described. **F** Volcano plot showing enriched PTM signatures in baseline versus post-treatment tumor samples via the PTM-SEA analysis. **G** Dose–response curve of relative proliferation of MDA-MB468 cells treated with paclitaxel and barasertib (Aurora kinase B inhibitor, 10 nM) plus paclitaxel in the *in-vitro* MTT assay. The x-axis is $\log_{10}$ (paclitaxel concentration). The results are from three biologic replicates, and the error bars indicate SEM. See also Figure S12. GSEA, gene set enrichment analysis; NMF, non-negative matrix factorization; pCR, pathological complete response; PTM, post-translational modification; TMT, tandem mass tag

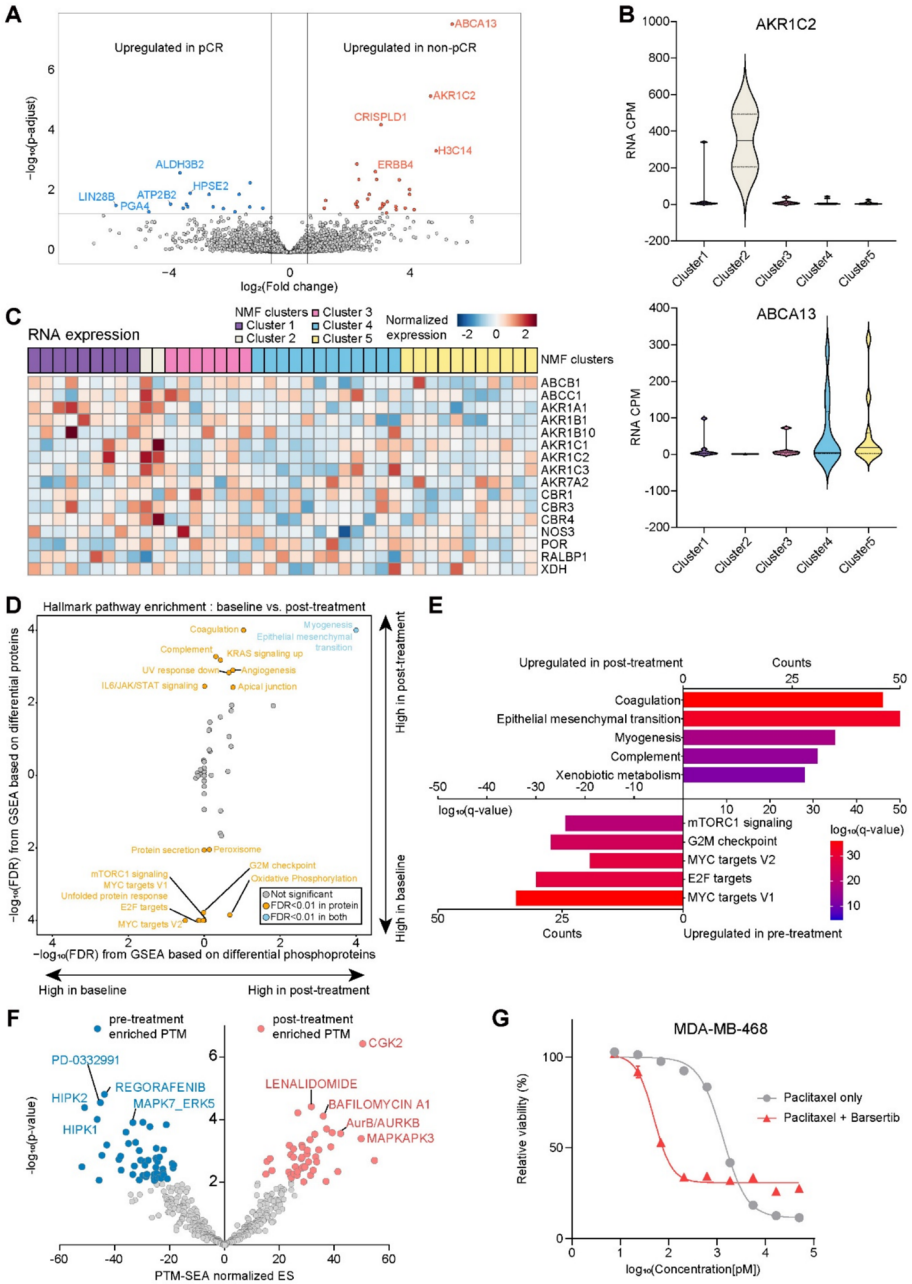

Fig. 5 (See legend on previous page.)

AURKB emerged as a particularly compelling target given its reported role in cell cycle regulation and chemotherapy resistance in TNBC [41, 42]. Functional validation in MDA-MB-468 cells demonstrated that the Aurora kinase B inhibitor barasertib significantly enhanced the cytotoxic effect of paclitaxel, supporting a synergistic interaction (Fig. 5G). Barasertib also decreased cell viability in doxorubicin-treated MDA-MB231 and HCC1937 TNBC cells (Additional file 1: Fig. S13A, B). In addition, barasertib decreased cell viability in combination with paclitaxel in a breast cancer organoid derived from a TNBC patient (SBO-72) (Additional file 1: Fig. S13C). These

findings suggest that AURKB is a therapeutic target to overcome residual disease and chemoresistance in patients with TNBC.

Proteogenomic biomarker prediction model for neoadjuvant chemotherapy response in patients with TNBC

We integrated proteogenomic predictive factors in patients with TNBC to constitute the prediction model for neoadjuvant chemotherapy. We used five resistance factors: estrogen response early signature (global protein level), GRK2 signature (PTM-SEA NES > 2), no *ITGB8* copy number loss (0 or 1 + in GISTIC), *AKR1C2* (RNA level), and *ABCA13* (RNA level). The expression levels of the five resistance factors did not differ according to the stroma proportion of tumor tissues and ESTIMATE stroma score (Additional file 1: Fig. S14). At least one resistance factor was identified in 80.7% of non-pCR patients (21 of 26; Fig. 6A), and 10 of these 21 patients had ≥ 2 resistance factors. In contrast, only 26.7% of pCR patients had one resistance factor. We generated the logistic regression model using continuous values for the five factors. In our proteogenomic prediction model, the AUC was 0.946, which was superior to that of the Lehmann classification (AUC = 0.781) or Lehmann classification plus the ESTIMATE immune score model (AUC = 0.818; Fig. 6B). Regarding individual cases, a 51-year-old woman (T39) with TNBC had three resistance factors (no *ITGB8* loss, high estrogen signature, and high *GRK2* signature) and showed progression on neoadjuvant paclitaxel/carboplatin chemotherapy (Fig. 6C). The patient underwent surgery and received adjuvant chemotherapy but had distant disease recurrence with lung metastasis 5 months post-surgery. Another 45-year-old woman (T47) with TNBC had one resistance factor (no *ITGB8* loss) and received neoadjuvant chemotherapy followed by surgery. The surgical tumor pathology showed non-pCR status, and capecitabine adjuvant chemotherapy was administered (Fig. 6D). She experienced distant disease recurrence 12 months post-surgery.

Discussion

TNBC tumors exhibit multifaceted heterogeneity across genomic, transcriptomic, and proteomic levels, compounded by the complexity of their tumor microenvironment, characterized by diverse immune and stromal interactions [1–3]. Previous molecular classification strategies predominantly utilized RNA profiling or DNA mutation signatures [4–6]. Alternatively, comprehensive proteogenomic analyses offer deeper biological insights, identifying previously unrecognized mechanisms of chemotherapy resistance. In this study, we prospectively collected paired baseline and post-treatment tumor samples from patients with TNBC treated with neoadjuvant chemotherapy. By integrating WES, RNA-seq, and TMT-based proteomic profiling data, we identified five distinct NMF clusters correlated with varying pCR rates, and these clusters did not overlap with the previously established Lehmann classification. The proteogenomic analysis highlighted novel resistance factors, including estrogen signaling, *GRK2* PTM signature activation, *ITGB8* copy number, and upregulation of drug-efflux and metabolism genes (*ABCA13* and *AKR1C2*). Using these identified proteogenomic features, we developed a predictive model for pCR following neoadjuvant chemotherapy. Additionally, AURKB emerged as a promising therapeutic target in residual tumors post-chemotherapy. These findings provide novel insights into the molecular determinants of chemotherapy

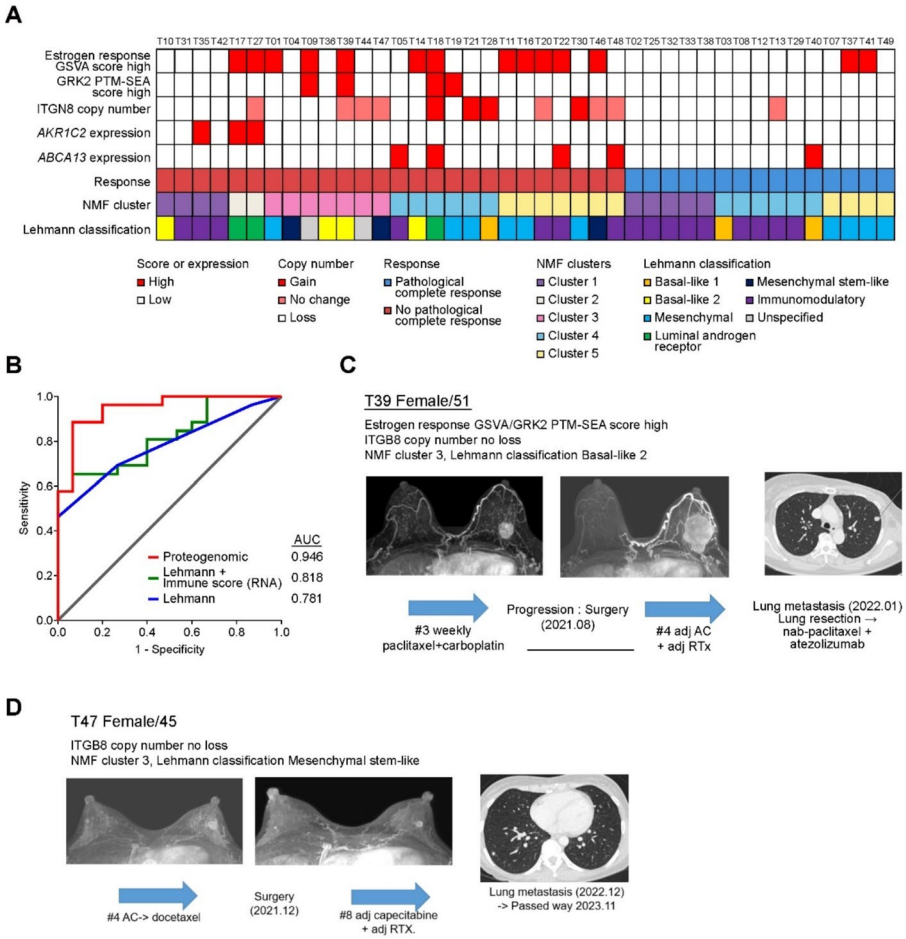

Fig. 6 Integration of proteogenomic biomarkers of predicting chemotherapy response in TNBC. **A** Heatmap summarizing the expression of key resistance-associated biomarkers, including estrogen response GSVA scores, GRK2 PTM-SEA scores, *ITGB8* copy number status, and *AKR1C2* and *ABCA13* expression across the TNBC cohort. Patients are annotated by pCR status, NMF cluster, and the Lehmann subtype classification. **B** Receiver operating characteristic curve comparing the predictive performance of the integrative proteogenomic model versus the RNA-based Lehmann classification for pCR. **C** Representative case highlighting clinical and molecular characteristics. This patient, classified as non-pCR, exhibited elevated estrogen response and GRK2 signaling and a diploid *ITGB8* copy number status and belonged to NMF Cluster 3 and the basal-like 2 Lehmann subtype. **D** A patient with TNBC who did not achieve pCR following neoadjuvant chemotherapy. This patient exhibited a diploid *ITGB8* copy number status and was classified as belonging to NMF Cluster 3 and the mesenchymal stem-like subtype based on the Lehmann classification. adj, adjuvant; AUC, area under curve; GSVA, gene set variation analysis; NMF, non-negative matrix factorization; PTM-SEA, post-translational modification set enrichment analysis

response in TNBC and support the integration of proteogenomic profiling into clinical strategies for response prediction and therapeutic targeting.

Integrating MS-based proteomics with RNA-seq and WES provides more comprehensive tumor characterization, adding protein-level expression data. Proteomics also uniquely captures PTMs, including protein phosphorylation profiles, which are undetectable by genomic or transcriptomic approaches. Krug et al. reported a proteogenomic analysis of breast cancers excavating more sophisticated molecular contexts regarding ERBB2 amplicon, RB activity, and DNA damage response [43]. However, dedicated proteogenomic studies of the TNBC subtype are few. Anurag et al. analyzed baseline tumor

samples of patients with TNBC receiving carboplatin and docetaxel neoadjuvant chemotherapy and identified *LIG1* deletion as a potential biomarker for poor chemotherapy response [25]. Gong and Jiang et al., analyzed proteogenomic landscape of TNBC and identified distinct targetable pathways according to the molecular subtypes (iCluster), including NAE1, FASN, and AKT signaling [28]. These two studies and our study performed mass spectrometry-based proteomic analysis and consistently found that activation of immune signature is related to pCR with favorable outcome and expression of EMT signature in TNBC clusters. Each study also uncovered unique resistance mechanisms—such as *LIG1* deletion, NAE1, and fatty-acid–metabolism (FASN/AKT) activation, and estrogen-signaling pathways. We suggest that differences in treatment settings (neoadjuvant versus adjuvant) and population-specific molecular features, including ethnic variation, may account for the observed discrepancies. The different clinical and molecular characteristics of Asian patients with breast cancer [44, 45] and different proportion of carboplatin use in the neoadjuvant chemotherapy regimens (Our study: 12% and Anurag et al.,: 100%) may have contributed to the differences between our study and that of Anurag et al. Distinctive aspects of our study include: (1) the focus on an Asian TNBC cohort, (2) investigation of anthracycline- and taxane-based neoadjuvant chemotherapy response, and (3) incorporation of both pre- and post-treatment tumor samples for longitudinal proteogenomic profiling.

Consistent with previous studies, our baseline analyses confirmed that immune-related signatures positively correlated with pCR, whereas EMT and myogenesis signatures negatively correlated [25, 46, 47]. Furthermore, our proteomic analysis uniquely identified protein estrogen response signatures to be significantly associated with non-pCR status. Considering the inverse correlation between estrogen and immune signatures, estrogen signaling in TNBC potentially hinders the anti-tumor immune response similar to that in hormone receptor-positive breast cancers [48]. Furthermore, we observed that estrogen-associated GRK2 activation correlates with chemotherapy resistance signatures, suggesting a possible role for this pathway that needs further validation. As all TNBC cases studied were negative for ER/PR via IHC, our findings emphasize the clinical relevance of detecting estrogen signaling through proteomic methods.

Frequent CNAs represent a hallmark of TNBC; however, their association with chemotherapy response remains unclear. Our analysis identified chromosome 7p21 CNAs to be significantly associated with treatment response. Specifically, the membrane integrin family protein ITGB8 exhibited the highest CNA difference between pCR and non-pCR tumors. Increased *ITGB8* copy number negatively correlated with pCR rates, and previous research suggested that ITGB8 facilitates immune evasion by promoting TGF-β signaling and subsequent suppression of CD8 + T-cell function [49]. We observed enhanced immune activation signatures in tumors with *ITGB8* loss compared to those in tumors with gain or diploid *ITGB8* copy number status, correlating with improved survival in TCGA cohorts. As ITGB8 and other integrins are expressed on the cancer cell membrane, they represent potential targets for developing antibody–drug conjugates. Accordingly, integrin beta protein-targeting antibody–drug conjugates are already under development for solid tumors [50].

Our study further highlights the significance of drug metabolism and efflux-related genes in chemotherapy resistance. The tumor-infiltrating lymphocyte density and

immune score of TNBC tumors correlate well with pCR after neoadjuvant chemotherapy [51, 52]. However, a small subset of the IM subtype TNBC still shows poor response to neoadjuvant chemotherapy. Increased expression of ABCA13 and AKR1C2 within the Lehmann IM subtype tumors was associated with neoadjuvant chemotherapy resistance. ABCA13 is a member of ATP-binding cassette transporters that regulate the efflux of chemotherapy drugs from cancer cells, causing multi-drug resistance. ABCA13 upregulation or amplification was associated with poor survival in ovarian and bladder cancers, and a study also reported poor survival of patients with breast cancer and single nucleotide polymorphism in *ABCA13* [39, 53, 54]. AKR1C2 belongs to the aldo–keto reductase family, which regulates xenobiotic and anthracycline metabolism. The role of the aldo–keto reductase family in chemotherapy resistance has been previously reported [55]. Our analysis also showed that AKR1C2 expression was upregulated in cluster 2, potentially causing resistance to cytotoxic chemotherapy.

Residual disease following neoadjuvant chemotherapy (non-pCR) significantly predicts poor prognosis [56, 57]. Our phosphoproteomic analysis revealed that AURKB, which is involved in cell division and TNBC pathogenesis, was notably upregulated at the PTM level in residual tumors. AURKB activation emerged as a key characteristic of residual TNBC, and our data suggest that targeting AURKB may synergize with paclitaxel therapy.

By leveraging the identified proteogenomic biomarkers—estrogen signaling, *GRK2* activation, *ITGB8* copy number status, and the expression of ABCA13 and AKR1C2—we developed an integrative predictive model for pCR that outperformed existing RNA-based approaches [58–60]. Currently, pembrolizumab plus cytotoxic chemotherapy, consisting of taxane/carboplatin followed by anthracycline and cyclophosphamide, represents the standard neoadjuvant therapy regimen for patients with stages II–III TNBC [15]. However, clinically validated pCR prediction biomarkers are lacking in patients with TNBC to date, and escalation and de-escalation of therapeutic modality are largely based on clinicopathologic characteristics including pCR status. Our proteogenomics-based predictive model could inform personalized treatment, potentially allowing therapeutic de-escalation and avoidance of toxic agents for responsive tumors while guiding targeted escalation strategies for resistant tumors.

The key strengths of this study include prospective collection of paired baseline and post-treatment samples with comprehensive multi-omics profiling—spanning RNA, DNA, and protein levels. Nonetheless, the findings should be interpreted cautiously given the relatively small sample size, and further validation in an independent proteogenomic cohort is warranted. Additionally, no patients in this study received pembrolizumab-based neoadjuvant chemotherapy owing to approval timelines in South Korea. Despite these limitations, our study provides valuable insight into molecular mechanisms underlying chemotherapy response, with potential applications for treating metastatic TNBC.

Conclusions

Our study demonstrates the utility of proteogenomic profiling to predict neoadjuvant chemotherapy response in TNBC. The key determinants of treatment outcome included estrogen response signature, *GRK2* PTM activation, *ITGB8* copy number, and

the expression of genes involved in drug efflux and metabolism, ABCA13 and AKR1C2. These factors constituted the non-pCR prediction model for neoadjuvant chemotherapy and may serve as potential molecular targets for future therapeutic development. Future clinical trials should investigate personalized neoadjuvant treatment strategies guided by proteogenomic markers to evaluate treatment escalation or de-escalation based on predicted response profiles.

Methods

Study design and participants

Fresh tumor biopsies were prospectively obtained from 50 patients diagnosed with clinical stage II–III TNBC defined as ER-, PR-, and HER2-negative (0 or 1 + by immunohistochemistry [IHC], or 2 + by IHC with a negative in-situ hybridization assay, CONSORT diagram in Additional file 1: Fig. S1) between September 2020 and July 2021. All baseline biopsy tissues were obtained before starting neoadjuvant chemotherapy. Patients received anthracycline and taxane-based neoadjuvant chemotherapy regimens. Neoadjuvant chemotherapy regimens were selected at the physician's discretion and included: AC (doxorubicin 60 mg/m^2 and cyclophosphamide 600 mg/m^2, four cycles)-weekly paclitaxel ($n = 36$, weekly paclitaxel 80 mg/m^2, 12 cycles), AC-docetaxel ($n = 6$, tri-weekly docetaxel 75 mg/m^2, four cycles), weekly paclitaxel plus carboplatin (area under the curve [AUC] 5, tri-weekly)-AC ($n = 6$), and FEC-docetaxel ($n = 2$). Only 44 patients completed the chemotherapy schedule, while six patients discontinued treatment due to disease progression. The pCR status at surgery was defined as ypT0 ypN0 determined by pathologic examination [61]. Post-treatment surgical tumor samples ($n = 31$) were collected and analyzed for participants who did not achieve pCR. This study was approved by the Institutional Review Board (IRB) of Severance Hospital (IRB Number: 4–2020-0473). The study for establishment of cancer organoids from TNBC patients was also approved by IRB of Severance Hospital (IRB Number: 4–2023-0098). This study adhered to the Declaration of Helsinki and Good Clinical Practice guidelines. The informed consents were obtained from all enrolled patients.

Tissue sampling and proteogenomic analysis

The sample collection and multiomic analysis methods used in this study have been described previously [62]. Briefly, frozen tissue samples were washed with cold phosphate-buffered saline, snap-frozen in liquid nitrogen, and pulverized using the cryoPREP Tissue Disruption system (CP02, Covaris, Woburn, MA, USA). Tissue powder aliquots (10–20 mg) were used for DNA, RNA, and protein extractions. Genomic DNA was extracted using the MagNA Pure 24 system (Roche, Basel, Switzerland), and total RNA was isolated using the RNeasy Mini Kit on a QIAcube (Qiagen, Hilden, Germany). Proteins were extracted and labeled with TMT 11-plex reagents. Across the dataset, the comprehensive proteogenomic analysis identified copy number alteration of 25,988 genes and the expression of 19,853 gene transcripts, 10,457 proteins, and 31,258 phosphorylation sites in 5,373 proteins. Full details regarding the proteogenomic sample preparation and analysis are provided in the Supplementary Methods.

Data quality control and differential expression and pathway enrichment analysis

The Wilcoxon rank sum test in R identified genes (RNA), proteins, phosphosites, and phosphoproteins (mean of all sites on a given protein) that differed between pCR and non-pCR samples. MSigDB Hallmark and C6 oncogenic pathways (proteomics data) and PTM signature sets (phosphosite-level data) that showed enrichment in pCR or non-pCR tumors were identified using Gene set enrichment analysis (GSEA) [63] and post-translational modification set enrichment analysis (PTM-SEA) [64], respectively, by applying GSEA/PTM-SEA algorithms to signed $\log_{10}$(p-values) from the differential expression analysis. Additionally, gene set variation analysis (GSVA) was conducted using the ssGSEA R package [65, 66], utilizing the RNA, protein, and phosphoprotein data, and scores for Hallmark pathways were obtained for individual samples. Normalized enrichment scores were utilized for visualization. The Wilcoxon signed rank test in R was used for paired differential analysis of on-treatment to baseline measurements for RNA, protein, and phosphoprotein data. The Lehmann transcriptomic subtypes were estimated by TNBCtype tool (https://www.vumc.org/pietenpol-lab/tools) [22]. The PAM50 model was applied to RNA-seq data to determine the representation of intrinsic subtypes [67].

Non-negative matrix factorization (NMF) clustering and multi-omics data integration

To define molecular subtypes within the TNBC cohort, we performed NMF clustering on an integrated multi-omics dataset derived from baseline tumor samples. The dataset comprised four continuous data modalities: CNAs, RNA expression, global protein expression, and phosphoprotein expression.

Preprocessing for each data modality was conducted as follows to ensure comparability and compatibility with NMF:

- Copy number alterations: Absolute copy number values obtained from GISTIC2 outputs were used to maintain non-negativity.
- RNA, protein, and phosphoprotein expression: Each dataset was independently normalized across samples to standardize dynamic ranges and distribution.
- Data integration: Because NMF requires non-negative input, a constant value was added to each normalized matrix. The four data matrices were concatenated by gene identifier to construct a unified feature matrix (features × samples).

Consensus NMF clustering was then applied using the "brunet" method for a range of clusters between k = 2 and 8 (rank = 2:8) with 50 iterations (nrun = 50) using the NMF R package (v 0.28) [68]. The optimal cluster number (k = 5) was selected based on cophenetic correlation coefficients, dispersion, and consensus clustering stability metrics.

Cell culture

The TNBC cell lines, including MDA-MB-231 (HTB-26), MDA-MB-468 (HTB-132), and HCC1937 (CRL-2336), were purchased from the ATCC. Cells were cultured at 37℃ in 5% CO_2 using the RPMI-1640 medium (Gibco, Thermo Fisher Scientific) and Dulbecco's Modified Eagle Medium supplemented with 10% fetal bovine serum (Gibco,

Thermo Fisher Scientific) and 1% penicillin–streptomycin (Gibco, Thermo Fisher Scientific). Doxorubicin (Sigma-Aldrich, St. Louis, MO, USA, cat# D1515) and carboplatin (Selleckchem, Houston, TX, USA, cat# S1215) were dissolved in distilled water, and the Aurora B kinase inhibitor (Barasertib, Selleckchem, cat# S1147) was dissolved in dimethyl sulfoxide (DMSO). β-estradiol (Sigma-Aldrich, cat# E2257) was dissolved in 100% ethanol and advanced DMEM/F-12 (Gibco, Thermo Fisher Scientific). All cell lines were authenticated by short tandem repeat profiling and were periodically tested for mycoplasma contamination.

Immunoblotting

For immunoblotting, cells were lysed using RIPA lysis buffer supplementation with protease and phosphatase inhibitor cocktails (Sigma Aldrich). The cell lysates were centrifuged for 10 min at 4 °C at 13,000 × g. Supernatants containing 10–40 μg protein were resolved by sodium dodecyl sulfate–polyacrylamide gel electrophoresis and transferred to nitrocellulose membranes. After blocking with 5% skim milk for 1 h at room temperature, each membrane was incubated overnight at 4 °C with primary antibodies. Subsequently, each membrane was incubated with secondary antibodies for 1 h at room temperature. The protein bands were detected by enhanced chemiluminescence (Amersham Biosciences, Uppsala, Sweden) using a luminescent image analyzer (LAS-3000, Fuji Photo Film, Tokyo, Japan). The following primary and secondary antibodies were used: GRK2 mouse (Santa Cruz Biotech, Santa Cruz, CA, USA, cat# sc-13143), β-actin rabbit (AbClon, Seoul, South Korea, cat# AbC-2002), and Anti-mouse IgG, HRP-linked Antibody (Enzo Life Sciences, Farmingdale, NY, USA, cat# ADI-SAB-100), Anti-rabbit IgG, HRP-linked Antibody (Enzo Life Sciences, cat# ADI-SAB-300).

Cell viability assay

TNBC cell lines (MDA-MB-231, MDA-MB-468, and HCC1937) were seeded at a density of 6×10^3 cells per well in 96-well plates to assess the synergistic effect of the drug combination. Cells were then treated with a combination of either a GRK2 inhibitor (βARK1 inhibitor, Sigma-Aldrich, 24269–96-3) or an Aurora B kinase inhibitor (barasertib, Selleckchem, Houston, TX, USA) and a concentration gradient of paclitaxel (0–50 nM) for 72 h. Cell viability was determined by measuring absorbance at 570 nm after incubation with 3-(4,5-dimethylthiazol-2-yl)−2,5-diphenyltetrazolium bromide (MTT) (5 mg/mL) for 2 h. The potential synergistic effect of the GRK2 inhibitor and paclitaxel was evaluated by assessing the cell viability of the MDA-MB-231 cell line through MTT assay after combination treatment with various concentrations of the GRK2 inhibitor and paclitaxel over 72 h, followed by analysis of the bliss synergy score using SynergyFinder 3.0 software.

cDNA Transfection

TNBC cell lines were transfected with a pEGFP-C2-entry plasmid or GFP-tagged human integrin β8 plasmid. Integrin β8-GFP was a gift from Bianxiao Cui (Addgene plasmid # 205093; http://n2t.net/addgene:205093; RRID: Addgene205093). Each parental cell line was seeded in a 6-well plate (Corning) at a density of 3–5 × 105 cells/well. When the cells reached 70–80% confluence, 1–2 μg of plasmid DNA was transfected into the cells

using Lipofectamine LTX (Thermo Fisher Scientific) according to the manufacturer's protocol. After 4 h, the medium was replaced with medium containing geneticin (G418, 0.4–1 mg/mL) (Thermo Fisher Scientific). G418 was used to select plasmid-transfected cells, which subsequently formed stable clones. Stable cell lines with a low passage number were cryopreserved and used in the experiments.

Drug treatment of breast cancer organoids

The breast cancer organoids were established from surgical tissues of patients with breast cancer in Yonsei Cancer Center, as previously reported [69]. Organoids were harvested and dissociated into single cells using TrypLE™ Express (Gibco). Cell pellets were resuspended in AdDF + + + medium (Advanced DMEM/F12 supplemented with 1 × GlutaMAX and 10 mM HEPES), followed by filtration through a 70-μm strainer. A total of 1.5×10^4 cells were embedded in 20 μl BME domes and seeded in 48-well plates. To assess pharmacologic interactions, breast cancer organoids were treated for 72 h with barasertib in combination with doxorubicin or carboplatin. Organoid viability was quantified using the CellTiter-Glo® 3D ATP assay (Promega).

3D culture and drug treatment

TNBC cell lines (MDA-MB-231 and MDA-MB-468) were seeded in BME2 (90%) at a density of 1×10^4 cells per well in 48-well plates and allowed to form organoids over 1–2 days. The media was supplemented with Type 2 medium. Type 2 organoid medium for 3D culture was formulated based on the composition previously reported [70], including supplementation with EGF, FGF-2, and B27, with Y-27632 (10 μM) added during the initial seeding period only. After 1–2 days of culture, the Y-27632 (ROCK inhibitor) was removed from the media, and the organoids were treated with paclitaxel or doxorubicin at the indicated concentrations for 3 days. To measure cell viability, culture medium was removed and 300ul fresh advanced DMEM/F12 medium was added to each well at day 3. Each well was treated with 150ul CellTiter-Glo® 3D (Promega, G9681) and incubated for 10 min. The mixture was transferred to 96-well white wall plates. Luminescence was recorded by BertholdTech CENTRO (Embedded version: 2.05).

Statistical analysis

Comparisons of continuous variables between groups were conducted using the Student's t-test. Correlations between two continuous variables were assessed using Pearson's correlation coefficient, with corresponding p-values and R^2 values reported. Overall survival of both the study cohort and The Cancer Genome Atlas (TCGA) dataset was estimated using Kaplan–Meier survival curves, and statistical significance was evaluated with the log-rank test. To develop a predictive model for non-pCR, logistic regression analysis was employed, incorporating selected proteogenomic biomarkers. The data analyses were performed using R version 4.3.1 (R Foundation for Statistical Computing), GraphPad Prism (GraphPad, La Jolla, CA, USA), SPSS (SPSS, Chicago, IL, USA) and GENE-E (Broad Institute, Cambridge, MA, USA). All p-values were calculated as two-sided, and significance was defined as $P < 0.05$.

Supplementary Information

The online version contains supplementary material available at https://doi.org/10.1186/s13059-026-04053-7.

Additional file 1: Supplementary methods, table, and figures in this study. Supplementary methods. Table S1. Baseline clinical characteristics of TNBC patients in this study. Fig S1. CONSORT diagram summarizing patient enrollment, treatment, and sample collection in the TNBC cohort. Fig S2. Overview of proteogenomic analysis, clinical outcomes, and pathway correlations in patients with TNBC. Fig S3. Comparison of NMF-defined proteogenomic clusters with Fudan TNBC classification. Fig S4. Gene set variation analysisof transcriptomic and proteomic profiles stratified by NMF clusters. Fig S5. External validation of the proteogenomic TNBC classification in the METABRIC cohort. Fig S6. Estrogen response gene signature across NMF clusters and correlation with immune and epithelial-to-mesenchymal transitionsignatures. Fig S7. External validation of resistance-associated biomarkers in independent TNBC proteogenomic datasets. Fig S8. Synergistic inhibition in MDA-MB231 cells with combined paclitaxel and GRK2inhibitor treatment. Fig S9. Chromosome-specific copy number, RNA, and protein expression patterns associated with pathologic response status in TNBC: Cytoband enrichment analysis by pCR and non-pCR groups. Fig S10. Integrin gene expression and immune contexture associated with chemotherapy response and ITGB8 copy number status in TNBC. Fig S11. Transcriptomic impact of ITGB8 overexpression in MDA-MB-468 TNBC cells. Fig S12. Proteomic and phosphoproteomic changes associated with chemotherapy resistance in TNBC. Fig S13. Cell viability assay of barasertib and chemotherapy combination treatment in TNBC cells. Fig S14. Assessment of stromal content and its effect on key resistance-associated factors in TNBC.

Additional file 2: Proteomic and phosphoproteomic data and dataset sources in this study. Table S2. Per-sample global protein abundance quantified by TMT-based proteomics. Table S3. Per-sample phosphoprotein abundance quantified by TMT-based proteomics. Table S4. Source of datasets used in this study.

Acknowledgements

The authors thank the patients, their families, and all investigators involved in this study. This work was done under the auspices of a Memorandum of Understanding between National Cancer Center of Korea (NCC) and the U.S. National Cancer Institute's International Cancer Proteogenome Consortium (ICPC). ICPC encourages international cooperation among institutions and nations in proteogenomic cancer research in which proteogenomic datasets are made available to the public. We thank Dr. Henry Rodriguez and Dr. Ana I. Robles from the U.S. National Cancer Institute's Clinical Proteomic Tumor Analysis Consortium (CPTAC) for helpful discussions.

Peer review information

Fengchao Yu and Tim Sands were the primary editors of this article and managed its editorial process and peer review in collaboration with the rest of the editorial team. The peer-review history is available in the online version of this article.

Authors' contributions

Conceptualization, M.H.K., G.M.K., J.B.P., S.P., and J.S.; methodology and validation, all authors; investigation, D.K.L., M.H.K., Y.H., S.K., W.R., G.K., H.Y., S.Y.P., J.D.L., H.J.H., G.M.K., K.K., J.B.P., M.J.K., J.S.K., J.Y.K., H.S.P., S.I.K., and H.Y.G.; visualization, D.K.L., M.H.K., and Y.H.; Funding acquisition, S.P. and J.S.; project administration, S.P. and J.S.; supervision: H.Y.G., S.P., and J.S.; writing – original draft, D.K.L., M.H.K., S.P., and J.S.; writing – review and editing, S.P. and J.S.

Funding

This work was supported by grants from the National Cancer Center, Korea (NCC-1810861), National Research Foundation of Korea (NRF) funded by the Korea government (MSIT) (RS-2024–00452509), the MD-PhD/Medical Scientist Training Program through the Korea Health Industry Development Institute, funded by the Ministry of Health & Welfare, Republic of Korea, the Korea Health Technology R&D Project through the Korea Health Industry Development Institute (KHIDI), funded by the Ministry of Health & Welfare, Republic of Korea (grant number: RS-2024–00439841 and RS-2025–25459146), and the National R&D Program for Cancer Control through the National Cancer Center (NCC) funded by the Ministry of Health & Welfare, Republic of Korea (HA22C0086). This study was also supported by a grant from the Handok Inc., Seoul, Republic of Korea, and the Handok Inc had no role in study design, data collection and analysis, decision to publish, or preparation of the manuscript.

Data availability

The sequencing datasets used in the primary analysis are available through NCBI Bioproject under accession numbers PRJNA1422845 (whole exome sequencing) [71] and PRJNA1422844 (RNA sequencing) [72]. Raw proteomic and phosphoproteomic mass spectrometry data have been deposited in the Proteomic Data Commons (PDC) under study identifiers PDC000695 (proteome) [73] and PDC000696 (phosphoproteome) [74]. The TMT-processed protein and phosphoprotein expression data are listed in Additional file 2: Table S2 (protein) and S3 (phosphoprotein). Third-party sequencing data [23, 25, 28, 38] used in this study are listed in Additional file 2: Table S4.

Declarations

Ethics approval and consent to participate

This study was approved by the Institutional Review Board (IRB) of Severance Hospital (IRB Number: 4–2020-0473) and adhered to the Declaration of Helsinki and Good Clinical Practice guidelines. The informed consents were obtained from all enrolled patients.

Consent for publication

Not applicable.

Competing interests
The authors declare no competing interests.

Author details
[1]Department of Pharmacology, Yonsei University College of Medicine, Seoul, Republic of Korea. [2]Division of Medical Oncology, Department of Internal Medicine, Yonsei Cancer Center, Yonsei University College of Medicine, 50-1 Yonsei-ro, Seodaemun-gu, Seoul 03722, Republic of Korea. [3]Avison Biomedical Research Center, Yonsei University College of Medicine, Seoul, Republic of Korea. [4]Division of Hematology and Oncology, Department of Internal Medicine, CHA Bundang Medical Center, CHA University, Seongnam, Republic of Korea. [5]Biopharmaceutical Chemistry Major, Department of Applied Chemistry, School of Science and Technology, Kookmin University, Seoul, Republic of Korea. [6]Department of Medicine, Kyung Hee University School of Medicine, Seoul, Republic of Korea. [7]Department of Radiology, Research Institute of Radiologic Science, Yonsei University College of Medicine, Seoul, Korea. [8]Department of Pathology, Yonsei University College of Medicine, Seoul, Korea. [9]Division of Breast Surgery, Department of Surgery, Yonsei Cancer Center, Yonsei University College of Medicine, 50-1 Yonsei-ro, Seodaemun-gu, Seoul 03722, Republic of Korea.

Received: 8 August 2025 Accepted: 20 March 2026
Published online: 14 April 2026

References

1. Foulkes WD, Smith IE, Reis-Filho JS. Triple-negative breast cancer. N Engl J Med. 2010;363:1938–48.
2. Dent R, Trudeau M, Pritchard KI, Hanna WM, Kahn HK, Sawka CA, et al. Triple-negative breast cancer: clinical features and patterns of recurrence. Clin Cancer Res. 2007;13:4429–34.
3. Zagami P, Carey LA. Triple negative breast cancer: pitfalls and progress. NPJ Breast Cancer. 2022;8:95.
4. Lehmann BD, Bauer JA, Chen X, Sanders ME, Chakravarthy AB, Shyr Y, et al. Identification of human triple-negative breast cancer subtypes and preclinical models for selection of targeted therapies. J Clin Invest. 2011;121:2750–67.
5. Burstein MD, Tsimelzon A, Poage GM, Covington KR, Contreras A, Fuqua SA, et al. Comprehensive genomic analysis identifies novel subtypes and targets of triple-negative breast cancer. Clin Cancer Res. 2015;21:1688–98.
6. Jiang YZ, Ma D, Suo C, Shi J, Xue M, Hu X, et al. Genomic and transcriptomic landscape of triple-negative breast cancers: subtypes and treatment strategies. Cancer Cell. 2019;35:428-440.e425.
7. Masuda H, Baggerly KA, Wang Y, Zhang Y, Gonzalez-Angulo AM, Meric-Bernstam F, et al. Differential response to neoadjuvant chemotherapy among 7 triple-negative breast cancer molecular subtypes. Clin Cancer Res. 2013;19:5533–40.
8. Emens LA, Molinero L, Loi S, Rugo HS, Schneeweiss A, Diéras V, et al. Atezolizumab and nab-paclitaxel in advanced triple-negative breast cancer: biomarker evaluation of the IMpassion130 study. J Natl Cancer Inst. 2021;113:1005–16.
9. Andre F, Ismaila N, Allison KH, Barlow WE, Collyar DE, Damodaran S, et al. Biomarkers for adjuvant endocrine and chemotherapy in early-stage breast cancer: ASCO guideline update. J Clin Oncol. 2022;40:1816–37.
10. Mayer IA, Zhao F, Arteaga CL, Symmans WF, Park BH, Burnette BL, et al. Randomized phase III postoperative trial of platinum-based chemotherapy versus capecitabine in patients with residual triple-negative breast cancer following neoadjuvant chemotherapy: ECOG-ACRIN EA1131. J Clin Oncol. 2021;39:2539–51.
11. Traina TA, Miller K, Yardley DA, Eakle J, Schwartzberg LS, O'Shaughnessy J, et al. Enzalutamide for the treatment of androgen receptor-expressing triple-negative breast cancer. J Clin Oncol. 2018;36:884–90.
12. Lehmann BD, Abramson VG, Sanders ME, Mayer EL, Haddad TC, Nanda R, et al. TBCRC 032 IB/II multicenter study: molecular insights to AR antagonist and PI3K inhibitor efficacy in patients with AR(+) metastatic triple-negative breast cancer. Clin Cancer Res. 2020;26:2111–23.
13. Li Y, Zhang H, Merkher Y, Chen L, Liu N, Leonov S, et al. Recent advances in therapeutic strategies for triple-negative breast cancer. J Hematol Oncol. 2022;15:121.
14. Liu Y, Hu Y, Xue J, Li J, Yi J, Bu J, et al. Advances in immunotherapy for triple-negative breast cancer. Mol Cancer. 2023;22:145.
15. Schmid P, Cortes J, Pusztai L, McArthur H, Kümmel S, Bergh J, et al. Pembrolizumab for early triple-negative breast cancer. N Engl J Med. 2020;382:810–21.
16. Schmid P, Cortes J, Dent R, Pusztai L, McArthur H, Kümmel S, et al. Event-free survival with pembrolizumab in early triple-negative breast cancer. N Engl J Med. 2022;386:556–67.
17. Korde LA, Somerfield MR, Carey LA, Crews JR, Denduluri N, Hwang ES, et al. Neoadjuvant chemotherapy, endocrine therapy, and targeted therapy for breast cancer: ASCO guideline. J Clin Oncol. 2021;39:1485–505.
18. Marra A, Curigliano G. Adjuvant and neoadjuvant treatment of triple-negative breast cancer with chemotherapy. Cancer J. 2021;27:41–9.
19. Mittendorf EA, Philips AV, Meric-Bernstam F, Qiao N, Wu Y, Harrington S, et al. Pd-l1 expression in triple-negative breast cancer. Cancer Immunol Res. 2014;2:361–70.
20. Telli ML, Timms KM, Reid J, Hennessy B, Mills GB, Jensen KC, et al. Homologous Recombination Deficiency (HRD) score predicts response to platinum-containing neoadjuvant chemotherapy in patients with triple-negative breast cancer. Clin Cancer Res. 2016;22:3764–73.
21. Sukumar J, Gast K, Quiroga D, Lustberg M, Williams N. Triple-negative breast cancer: promising prognostic biomarkers currently in development. Expert Rev Anticancer Ther. 2021;21:135–48.
22. Lehmann BD, Jovanović B, Chen X, Estrada MV, Johnson KN, Shyr Y, et al. Refinement of triple-negative breast cancer molecular subtypes: implications for neoadjuvant chemotherapy selection. PLoS One. 2016;11:e0157368.
23. Pereira B, Chin SF, Rueda OM, Vollan HK, Provenzano E, Bardwell HA, et al. The somatic mutation profiles of 2,433 breast cancers refines their genomic and transcriptomic landscapes. Nat Commun. 2016;7:11479.
24. Loi S, Drubay D, Adams S, Pruneri G, Francis PA, Lacroix-Triki M, et al. Tumor-infiltrating lymphocytes and prognosis: a pooled individual patient analysis of early-stage triple-negative breast cancers. J Clin Oncol. 2019;37:559–69.

25. Anurag M, Jaehnig EJ, Krug K, Lei JT, Bergstrom EJ, Kim BJ, et al. Proteogenomic markers of chemotherapy resistance and response in triple-negative breast cancer. Cancer Discov. 2022;12:2586–605.
26. Chakraborty B, Byemerwa J, Shepherd J, Haines CN, Baldi R, Gong W, et al. Inhibition of estrogen signaling in myeloid cells increases tumor immunity in melanoma. J Clin Invest. 2021;131:23.
27. Yoshihara K, Shahmoradgoli M, Martínez E, Vegesna R, Kim H, Torres-Garcia W, et al. Inferring tumour purity and stromal and immune cell admixture from expression data. Nat Commun. 2013;4:2612.
28. Gong TQ, Jiang YZ, Shao C, Peng WT, Liu MW, Li DQ, et al. Proteome-centric cross-omics characterization and integrated network analyses of triple-negative breast cancer. Cell Rep. 2022;38:110460.
29. Ansonoff MA, Etgen AM. Estrogen increases G protein coupled receptor kinase 2 in the cortex of female rats. Brain Res. 2001;898:186–9.
30. Nogués L, Reglero C, Rivas V, Salcedo A, Lafarga V, Neves M, et al. G protein-coupled receptor kinase 2 (GRK2) promotes breast tumorigenesis through a HDAC6-Pin1 axis. EBioMedicine. 2016;13:132–45.
31. Zimmerli D, Brambillasca CS, Talens F, Bhin J, Linstra R, Romanens L, et al. MYC promotes immune-suppression in triple-negative breast cancer via inhibition of interferon signaling. Nat Commun. 2022;13:6579.
32. Giuli MV, Giuliani E, Screpanti I, Bellavia D, Checquolo S. Notch signaling activation as a hallmark for triple-negative breast cancer subtype. J Oncol. 2019;2019:8707053.
33. Zhang K, Liu P, Tang H, Xie X, Kong Y, Song C, et al. AFAP1-AS1 promotes epithelial-mesenchymal transition and tumorigenesis through Wnt/β-catenin signaling pathway in triple-negative breast cancer. Front Pharmacol. 2018;9:1248.
34. Hu Z, Yuan J, Long M, Jiang J, Zhang Y, Zhang T, et al. The cancer surfaceome atlas integrates genomic, functional and drug response data to identify actionable targets. Nat Cancer. 2021;2:1406–22.
35. Boucard-Jourdin M, Kugler D, Endale Ahanda ML, This S, De Calisto J, Zhang A, et al. β8 integrin expression and activation of TGF-β by intestinal dendritic cells are determined by both tissue microenvironment and cell lineage. J Immunol. 2016;197:1968–78.
36. Takasaka N, Seed RI, Cormier A, Bondesson AJ, Lou J, Elattma A, et al. Integrin αvβ8-expressing tumor cells evade host immunity by regulating TGF-β activation in immune cells. JCI Insight. 2018;3:e122591.
37. Lainé A, Labiad O, Hernandez-Vargas H, This S, Sanlaville A, Léon S, et al. Regulatory T cells promote cancer immune-escape through integrin αvβ8-mediated TGF-β activation. Nat Commun. 2021;12:6228.
38. Ciriello G, Gatza ML, Beck AH, Wilkerson MD, Rhie SK, Pastore A, et al. Comprehensive molecular portraits of invasive lobular breast cancer. Cell. 2015;163:506–19.
39. Nymoen DA, Holth A, Hetland Falkenthal TE, Tropé CG, Davidson B. CIAPIN1 and ABCA13 are markers of poor survival in metastatic ovarian serous carcinoma. Mol Cancer. 2015;14:44.
40. Heibein AD, Guo B, Sprowl JA, Maclean DA, Parissenti AM. Role of aldo-keto reductases and other doxorubicin pharmacokinetic genes in doxorubicin resistance, DNA binding, and subcellular localization. BMC Cancer. 2012;12:381.
41. Jalalirad M, Haddad TC, Salisbury JL, Radisky D, Zhang M, Schroeder M, et al. Aurora-A kinase oncogenic signaling mediates TGF-β-induced triple-negative breast cancer plasticity and chemoresistance. Oncogene. 2021;40:2509–23.
42. Ratinho L, Meyer N, Greive S, Cressiot B, Pelta J. Nanopore sensing of protein and peptide conformation for point-of-care applications. Nat Commun. 2025;16:3211.
43. Krug K, Jaehnig EJ, Satpathy S, Blumenberg L, Karpova A, Anurag M, et al. Proteogenomic landscape of breast cancer tumorigenesis and targeted therapy. Cell. 2020;183:1436-1456.e1431.
44. Leong SPL, Shen ZZ, Liu TJ, Agarwal G, Tajima T, Paik N-S, et al. Is breast cancer the same disease in Asian and Western countries? World J Surg. 2010;34:2308–24.
45. Takahashi M, Cortés J, Dent R, Pusztai L, McArthur H, Kümmel S, et al. Pembrolizumab plus chemotherapy followed by pembrolizumab in patients with early triple-negative breast cancer: a secondary analysis of a randomized clinical trial. JAMA Netw Open. 2023;6:e2342107.
46. van den Ende NS, Nguyen AH, Jager A, Kok M, Debets R, van Deurzen CHM. Triple-negative breast cancer and predictive markers of response to neoadjuvant chemotherapy: a systematic review. Int J Mol Sci. 2023;24:2969.
47. Błaszczak E, Miziak P, Odrzywolski A, Baran M, Gumbarewicz E, Stepulak A. Triple-negative breast cancer progression and drug resistance in the context of epithelial-mesenchymal transition. Cancers (Basel). 2025;17:228.
48. Treeck O, Schüler-Toprak S, Ortmann O. Estrogen actions in triple-negative breast cancer. Cells. 2020;9:2358.
49. Malenica I, Adam J, Corgnac S, Mezquita L, Auclin E, Damei I, et al. Integrin-α(V)-mediated activation of TGF-β regulates anti-tumour CD8 T cell immunity and response to PD-1 blockade. Nat Commun. 2021;12:5209.
50. Lyon RP, Jonas M, Frantz C, Trueblood ES, Yumul R, Westendorf L, et al. SGN-B6A: a new vedotin antibody-drug conjugate directed to integrin beta-6 for multiple carcinoma indications. Mol Cancer Ther. 2023;22:1444–53.
51. Denkert C, von Minckwitz G, Darb-Esfahani S, Lederer B, Heppner BI, Weber KE, et al. Tumour-infiltrating lymphocytes and prognosis in different subtypes of breast cancer: a pooled analysis of 3771 patients treated with neoadjuvant therapy. Lancet Oncol. 2018;19:40–50.
52. Martín M, Stecklein SR, Gluz O, Villacampa G, Monte-Millán M, Nitz U, et al. TNBC-DX genomic test in early-stage triple-negative breast cancer treated with neoadjuvant taxane-based therapy. Ann Oncol. 2025;36:158–71.
53. Pichler R, Lindner AK, Compérat E, Obrist P, Schäfer G, Todenhöfer T, et al. Amplification of 7p12 is associated with pathologic nonresponse to neoadjuvant chemotherapy in muscle-invasive bladder cancer. Am J Pathol. 2020;190:442–52.
54. Hlaváč V, Václavíková R, Brynychová V, Koževnikovová R, Kopečková K, Vrána D, et al. Role of genetic variation in ABC transporters in breast cancer prognosis and therapy response. Int J Mol Sci. 2020;21:9556.
55. Li S, Lee W, Heo W, Son HY, Her Y, Kim JI, et al. AKR1C2 promotes metastasis and regulates the molecular features of luminal androgen receptor subtype in triple negative breast cancer cells. J Breast Cancer. 2023;26:60–76.
56. Hamy AS, Darrigues L, Laas E, De Croze D, Topciu L, Lam GT, et al. Prognostic value of the residual cancer burden index according to breast cancer subtype: validation on a cohort of BC patients treated by neoadjuvant chemotherapy. PLoS One. 2020;15:e0234191.
57. Yau C, Osdoit M, van der Noordaa M, Shad S, Wei J, de Croze D, et al. Residual cancer burden after neoadjuvant chemotherapy and long-term survival outcomes in breast cancer: a multicentre pooled analysis of 5161 patients. Lancet Oncol. 2022;23:149–60.

58. Echavarria I, López-Tarruella S, Picornell A, García-Saenz J, Jerez Y, Hoadley K, et al. Pathological response in a triple-negative breast cancer cohort treated with neoadjuvant carboplatin and docetaxel according to Lehmann's refined classification. Clin Cancer Res. 2018;24:1845–52.
59. Zhang W, Li E, Wang L, Lehmann BD, Chen XS. Transcriptome meta-analysis of triple-negative breast cancer response to neoadjuvant chemotherapy. Cancers (Basel). 2023;15:2194.
60. Supplitt S, Karpinski P, Sasiadek M, Laczmanski L, Kujawa D, Matkowski R, et al. The analysis of transcriptomic signature of TNBC-searching for the potential RNA-based predictive biomarkers to determine the chemotherapy sensitivity. J Appl Genet. 2025;66:171–82.
61. Litton JK, Regan MM, Pusztai L, Rugo HS, Tolaney SM, Garrett-Mayer E, et al. Standardized definitions for efficacy end points in neoadjuvant breast cancer clinical trials: NeoSTEEP. J Clin Oncol. 2023;41:4433–42.
62. Kim KH, Migliozzi S, Koo H, Hong JH, Park SM, Kim S, et al. Integrated proteogenomic characterization of glioblastoma evolution. Cancer Cell. 2024;42:358-377.e358.
63. Subramanian A, Tamayo P, Mootha VK, Mukherjee S, Ebert BL, Gillette MA, et al. Gene set enrichment analysis: a knowledge-based approach for interpreting genome-wide expression profiles. Proc Natl Acad Sci U S A. 2005;102:15545–50.
64. Krug K, Mertins P, Zhang B, Hornbeck P, Raju R, Ahmad R, et al. A curated resource for phosphosite-specific signature analysis. Mol Cell Proteomics. 2019;18:576–93.
65. Barbie DA, Tamayo P, Boehm JS, Kim SY, Moody SE, Dunn IF, et al. Systematic RNA interference reveals that oncogenic KRAS-driven cancers require TBK1. Nature. 2009;462:108–12.
66. Hänzelmann S, Castelo R, Guinney J. GSVA: gene set variation analysis for microarray and RNA-seq data. BMC Bioinformatics. 2013;14:7.
67. Parker JS, Mullins M, Cheang MC, Leung S, Voduc D, Vickery T, et al. Supervised risk predictor of breast cancer based on intrinsic subtypes. J Clin Oncol. 2009;27:1160–7.
68. Gaujoux R, Seoighe C. A flexible R package for nonnegative matrix factorization. BMC Bioinformatics. 2010;11:367.
69. Ryu WJ, Park S, Lee JD, Hwang Y, Jo S, Yong KT, et al. Abstract 178: establishment of patient-derived organoid of breast cancer. Cancer Res. 2023;83:178–178.
70. Dekkers JF, van Vliet EJ, Sachs N, Rosenbluth JM, Kopper O, Rebel HG, et al. Long-term culture, genetic manipulation and xenotransplantation of human normal and breast cancer organoids. Nat Protoc. 2021;16:1936–65.
71. Lee DK KM, Hwang Y, Kim S-G, Ryu W-J, Kim G-U, Yun HM, Park SY, Lee JD, Han HJ, Kim GM, Kim K-H, Park JB, Kim MJ, Koo JS, Kim JY, Park HS, Kim SI, Gee HY, Park S, Sohn J: Triple-negative breast cancer WES. PRJNA1422845. 2026. https://www.ncbi.nlm.nih.gov/bioproject/?term=PRJNA1422845.
72. Lee DK KM, Hwang Y, Kim S-G, Ryu W-J, Kim G-U, Yun HM, Park SY, Lee JD, Han HJ, Kim GM, Kim K-H, Park JB, Kim MJ, Koo JS, Kim JY, Park HS, Kim SI, Gee HY, Park S, Sohn J: Triple-negative breast cancer RNA sequencing. PRJNA1422844. 2026. https://www.ncbi.nlm.nih.gov/bioproject/?term=PRJNA1422844.
73. Lee DK KM, Hwang Y, Kim S-G, Ryu W-J, Kim G-U, Yun HM, Park SY, Lee JD, Han HJ, Kim GM, Kim K-H, Park JB, Kim MJ, Koo JS, Kim JY, Park HS, Kim SI, Gee HY, Park S, Sohn J: Triple-negative breast cancer proteome. PDC000695. 2026. https://pdc.cancer.gov/pdc/study/PDC000695.
74. Lee DK KM, Hwang Y, Kim S-G, Ryu W-J, Kim G-U, Yun HM, Park SY, Lee JD, Han HJ, Kim GM, Kim K-H, Park JB, Kim MJ, Koo JS, Kim JY, Park HS, Kim SI, Gee HY, Park S, Sohn J: Triple-negative breast cancer phosphoproteome. PDC000696. 2026. https://pdc.cancer.gov/pdc/study/PDC000696.

Publisher's Note